

We are IntechOpen, the world's leading publisher of Open Access books Built by scientists, for scientists

6,400

Open access books available

173,000

International authors and editors

190M

Downloads

Our authors are among the

154

Countries delivered to

TOP 1%

most cited scientists

12.2%

Contributors from top 500 universities



WEB OF SCIENCE™

Selection of our books indexed in the Book Citation Index
in Web of Science™ Core Collection (BKCI)

Interested in publishing with us?
Contact book.department@intechopen.com

Numbers displayed above are based on latest data collected.
For more information visit www.intechopen.com



Soil moisture estimation using L-band radiometry

Alessandra Monerris¹ and Thomas Schmugge²

¹*Remote Sensing Laboratory, TSC-UPC, and SMOS-BEC, Barcelona, Spain*

²*Physical Sciences Laboratory, New Mexico State University, Las Cruces, NM, USA*

1. Introduction

About 70% of the Earth is covered with water, 97% of which is part of oceans. Heating of oceans by the Sun keeps the Earth's water in a continuous circulation from the atmosphere to the Earth and back to the atmosphere through condensation, evapotranspiration, and precipitation processes. This continuous water motion is called water cycle. The groundwater in the unsaturated or vadose zone of land is usually referred to as soil moisture. The thickness of this zone extends from soil surface to a few metres below the surface in humid regions, and to 300 m or more below surface in arid regions. Although the water held by soils is a small fraction of the Earth's water budget, soil moisture plays an important role in the water cycle since it controls the proportion of rainfall that percolates, runs off, or evaporates from the land, influences plants growth and transpiration, and is related to the precipitation variability within a region (Koster et al., 2004).

Although soil moisture is one of the main parameters used in climate models, because of the large temporal and spatial variations of soil moisture sparse in-situ measurements are inadequate to be of much use in these models. Remote sensing with sufficient accuracy would provide meaningful soil moisture data over large regions. The maximum sensitivity to soil moisture is achieved in the lower range of microwave frequencies, which goes from 1 to 5 GHz (wavelength from 30 cm to 5 cm, respectively). The justification to this behaviour can be found if the dielectric properties of a target are analysed, since they have a large influence on its microwave brightness temperature. Land surfaces can be considered as a mixture of soil, water, and air particles and thus soil moisture might be estimated from measurements if the contrast between the water and soil particles were large enough. At microwave frequencies the real part of dry soil and water dielectric constants are approximately 4 and 80, respectively (Jackson & Schmugge, 1989). The scientific literature concluded that microwave radiometry at L-band (1.4-1.427 GHz) is optimal to estimate soil moisture, not only because it is very sensitive to soil moisture, but also because provides all-weather coverage, since the atmosphere at microwave frequencies may be considered nearly transparent, and vegetation is semi-transparent, which allows observations of the underlying layers (Eagleman, 1976; Wang & Choudhury, 1981; Jackson & Schmugge 1991). This specific band was chosen because it is a radio astronomy quiet band.

1.1. Satellite missions for soil moisture estimation using passive microwave sensors

While L-band microwave sensors provide maximum sensitivity to soil moisture their long wavelength implies the need for large antennae to achieve useful spatial resolution. For example, to obtain a ground resolution of 50 km or less using classical solutions on low-orbit satellites implies an antenna size of up to 20 m. At present, different scientific groups are developing new techniques to face this problem, and two space missions have been proposed to measure soil moisture at global scale: ESA's SMOS and NASA's SMAP.

The Soil Moisture and Ocean Salinity mission

The Soil Moisture and Ocean Salinity (SMOS) mission will observe soil moisture over land and salinity over oceans, and will measure snow and ice areas contributing to studies of the cryosphere (Kerr et al., 2001; Barré et al., 2008). Scheduled for launch in autumn 2009, it is the second Earth Explorer mission and part of ESA's Living Planet Programme. SMOS was thought of as a cost-effective, demonstrator mission with a nominal (extended) lifetime of 3 (5) years. The orbit is quasi-circular, sun-synchronous and dawn-dusk, and will be in the low-Earth range, at 763 km.

The SMOS mission provides a completely new approach in the field of remote sensing at L-band. Its payload MIRAS (Microwave Radiometer by Aperture Synthesis) is the first-ever two-dimensional interferometric radiometer in space. MIRAS consists of a Y-shaped antenna array with three arms, each arm having an approximate length of 4.5 m and 21 dual-polarisation L-band antennae or LICEF (Light Cost Effective Front-end) spaced 0.875 times the wavelength. Each LICEF is a total power radiometer in its own. Nine redundant antenna and three full-polarimetric noise injection radiometers are located in a fixed structure in the centre of the array, while the arms are divided in three segments to be folded during the launch (McMullan et al., 2008). If classical solutions would have been used, with this antenna size and orbit altitude the field of view (FOV) would be of near 3000 km in diameter. However, because of the microwave interferometry technique, the instrument Y-shape and the antenna spacing, the resulting FOV is a hexagonal-like area of less than 1000 km (see Figure 1). The spatial resolution varies from 35 km at the FOV centre to 50 km at the border. MIRAS will provide observations of a single azimuth at various incidence angles (from 0° to 55°) and radiometric resolutions depending on its position within the field of view during a satellite overpass. This fact will much improve the retrieval algorithms because a lot of independent information of each pixel will be registered, and will permit the estimation of soil roughness, vegetation opacity and albedo, etc. together with soil moisture.

To satisfy the scientific requirements, SMOS aims at providing global maps of soil moisture every 3 days with a ground resolution better than 50 km, and a 0.04 m³/m³ volumetric humidity. This soil moisture accuracy is referred to pixels outside mountainous, urban, and partially frozen or snow-covered areas. For sea salinity, maps with accuracy better than 1.2 psu and 200 km ground resolution will be acquired every 30 days.

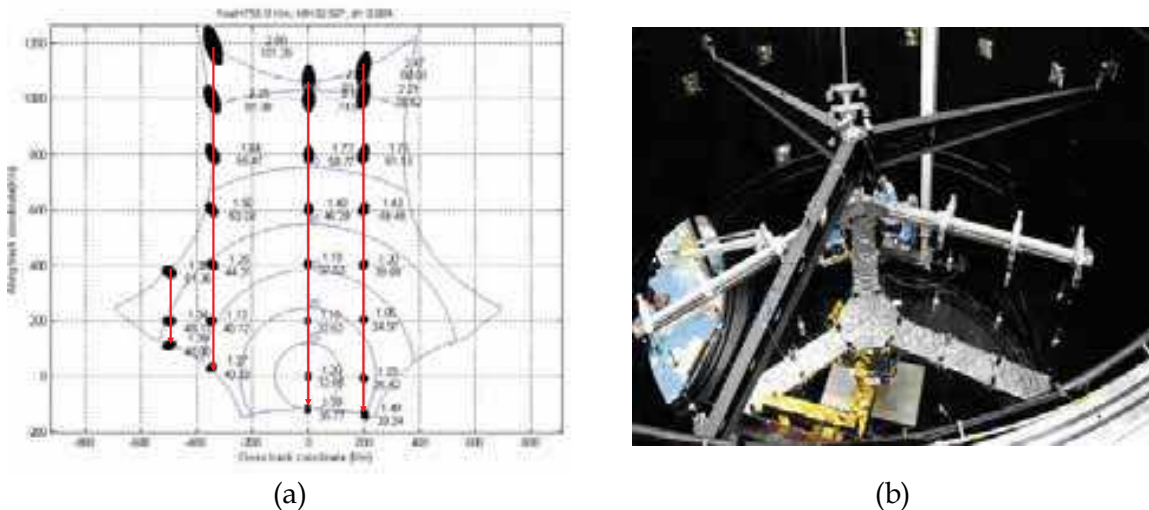


Fig. 1. (a) SMOS field of view. Blue lines indicate the observation angle, black ellipses indicate the pixel size depending on the position within the snap-shot, and red lines show how a single pixel can be observed under different viewing positions during a satellite overpass. (b) MIRAS during the IVT campaign at ESA-ESTEC Maxwell anechoic chamber premises (picture courtesy of EADS-CASA Espacio)

The Soil Moisture Active and Passive mission

The Hydrosphere State (HYDROS) mission was proposed by NASA to enhance the understanding of the land hydrosphere state and improve the climate prediction models (Entekhabi et al., 2004). The mission had a circular, polar, sun-synchronous, 6 am/pm equator crossing orbit located at 670 km altitude. Hydros aimed at providing soil moisture estimates with a 4% volumetric accuracy in the top 2-5 cm and capturing freeze/thaw state transitions in integrated vegetation-soil continuum at the spatial scale of landscape variability (3 km). The payload consisted of both active and passive sensors. An L-band radiometer measured the first, second, and third Stokes parameters with a 40 km spatial resolution, and 1 K relative accuracy, while an L-band radar acquired VV, HH, and HV polarisations with a 10 km resolution, and 0.5 dB accuracy for VV and HH. Observations at a constant incidence angle between 35° and 50°. Both the radar and the radiometer share a 6 m diameter reflector antenna which rotates about its nadir axis. The HYDROS mission was cancelled in 2005, but many HYDROS science and technology issues are being reviewed to be implemented in the future Soil Moisture Active and Passive (SMAP) mission.

1.2. Scope of this chapter

Space missions for Earth observation require a huge amount of previous work to validate the existing science and technology. This is accomplished through airborne and ground-based field experiments. This chapter reviews the basics of microwave radiometry and the existing models of soil emissivity and soil dielectric constant. The field experiments over land carried out during the last three decades are summarised, paying special attention to the recent experiments carried out by the Remote Sensing Laboratory from the Universitat Politècnica de Catalunya (UPC) as part of the preparatory activities for the SMOS mission over land.

2. L-band emission of land covers

Microwave remote sensing is based on the measurement of the thermal radiation or brightness temperature of a target, which is determined by its physical temperature and emissivity. The emissivity of land covers depends on soil moisture, but also on soil temperature (Choudhury et al., 1982; Wigneron et al., 2001), soil surface roughness (Mo & Schmugge, 1987; Escorihuela et al., 2007), vegetation canopy (Jackson & Schmugge, 1991; Ferrazzoli et al., 2002), snow cover (Schwank et al., 2004), relief (Mätzler & Standley, 2000; Talone et al., 2007), etc.

2.1. Soil dielectric constant model

The dielectric constant determines the response of the soil to an incident electromagnetic wave. This response is composed of two parts, real and imaginary ($\epsilon = \epsilon' + j\epsilon''$) which determine the wave velocity and energy losses respectively. In a non-homogeneous medium such as soils, the dielectric properties have a strong impact on its microwave emission. However, the relationship between the soil dielectric constant and the soil physical properties is not straightforward. A large number of studies have been performed during the last decades to find out this relationship since it plays an important part in the soil moisture retrieval algorithms from remote sensing data (Hipp, 1974; Wang & Schmugge, 1980; Topp et al., 1980; Hallikainen et al., 1985; Dobson et al., 1985; Roth et al., 1992; Mironov et al., 2004). Some of these models are simple empirical models in which data is fitted by a curve unique for all soils; others propose semi-empirical approaches which take into account some soil physical properties. The dielectric constant of dry soils is almost independent of temperature (Topp et al., 1980) and frequency. On the contrary, wet soils show a complex behaviour depending on the interaction between soil, water, and air particles. Hallikainen et al. (1985) performed a series of dielectric constant measurements of five soils with different texture composition at frequencies between 1.4 and 18 GHz and found out that texture has a strong effect on the dielectric behaviour which is specially pronounced at frequencies below 5 GHz.

In the dielectric-mixing model by Roth et al. (1992), differences in soil texture and bound water and free water are ignored altogether. Other models use a semi-empirical approach that contains a model of the complex dielectric constant and the volume fraction of each of the soil components. This kind of approach was followed by two widely used models presented in Wang & Schmugge (1980) and Dobson et al. (1985). The starting point of both of them is the dielectric mixing model by (Birchak et al., 1974),

$$\epsilon^\alpha = V_s \epsilon_s^\alpha + V_a \epsilon_a^\alpha + V_{fw} \epsilon_{fw}^\alpha + V_{bw} \epsilon_{bw}^\alpha, \quad (1)$$

where V_s (ϵ_s), V_a (ϵ_a), V_{fw} (ϵ_{fw}) and V_{bw} (ϵ_{bw}) are the volume fraction (dielectric constant) of solid phase, air, free water, and bound water in the soil, respectively. The expression in (1) can be rewritten as a function of the bulk density ρ_b , the particle density ρ_s , and the volumetric moisture m_v as

$$\epsilon^\alpha = 1 + \frac{\rho_b}{\rho_s} (\epsilon_s^\alpha - 1) + V_{fw} \epsilon_{fw}^\alpha + V_{bw} \epsilon_{bw}^\alpha - m_v. \quad (2)$$

The Wang & Schmugge (1980) model was proposed for 1.4 and 5 GHz frequencies and starts from (2) with $\alpha=1$. This model provides separate dielectric constant equations for volumetric water content lower than or greater than the transition moisture w_t . The transition moisture is the moisture content at which the free water phase begins to dominate the soil hydraulics, and it is strongly dependent on texture. The soil dielectric constant is then estimated as

$$\varepsilon = \begin{cases} m_v \varepsilon_x + (P - m_v) \varepsilon_a + (1 - P) \varepsilon_r, & m_v < w_t \\ w_t \varepsilon_x + (m_v - w_t) \varepsilon_{fw} + (P - m_v) \varepsilon_a + (1 - P) \varepsilon_r, & m_v > w_t \end{cases} \quad (3)$$

with

$$\varepsilon_x = \begin{cases} \varepsilon_i + (\varepsilon_{fw} - \varepsilon_i) \frac{m_v}{w_t} \gamma, & m_v < w_t \\ \varepsilon_i + (\varepsilon_{fw} - \varepsilon_i) \gamma, & m_v > w_t \end{cases} \quad (4)$$

and $\gamma = -0.57w_t + 0.481$, ε_i , ε_a , ε_{fw} , and ε_r the dielectric constants of ice, air, free water, and rock, respectively, ε_x the dielectric constant of the initially adsorbed water, and P the soil porosity. The variable ε_{fw} is estimated using the Debye equation.

On the other hand, the Dobson et al. (1985) model starts from (2) and assumes that there is not distinction between bound and free water. Taking this into account, the new expression for the dielectric constant is

$$\varepsilon = \left(1 + \frac{\rho_b}{\rho_s} (\varepsilon_s^\alpha - 1) + m_v^\beta \varepsilon_{fw}^\alpha - m_v \right)^{1/\alpha} \quad (5)$$

The real and imaginary parts of the dielectric constant of soils are obtained separately using the percentage of sand S and clay C in the soil, and $\beta = (127.48 - 0.519S - 0.152C)/100$ for the real part, and $\beta = (1.33979 - 0.603S - 0.166C)/100$ for the imaginary part. For further information on dielectric constant models refer to Behari (2005) and Chukhlantsev (2006).

2.2. Emission from bare soils

The emissivity of bare soils e_s is given by

$$\Gamma_{s,p} = 1 - e_{s,p} \quad (6)$$

where $\Gamma_{s,p}$ is the total reflectivity at p polarisation in a chosen observation direction, which can be expressed in terms of the bistatic scattering coefficients σ_{pp} and σ_{pq} as follows (Fung, 1994):

$$\Gamma_{s,p}(\theta_i, \varphi_i) = \frac{1}{4\pi} \int_{4\pi} [\sigma_{pp}(\theta_i, \varphi_i, \theta_r, \varphi_r) + \sigma_{pq}(\theta_i, \varphi_i, \theta_r, \varphi_r)] d\Omega_r \quad (7)$$

Subscripts i and r stand for the incident and scattered radiation, and θ and φ are the incidence and azimuth angles, respectively. The coefficient σ_{pp} , often called coherent component, considers the scattering on the observation direction and polarisation, while σ_{pq} , or incoherent component, considers the scattering in whatever other direction and

polarisation. The integration over the entire half space and errors in the modelling of the bistatic scattering coefficients make the computation of (7) unfeasible or prone to errors. For this reason, the uniform half space model with smooth surface is commonly adopted. This model is simpler and thus suitable to be used in soil moisture retrieval algorithms from remotely sensed data. In this case, the total reflectivity in (7) equals the reflection coefficient given by the Fresnel formulation.

Soil brightness temperature is related to soil emission through the soil effective temperature, T_{eff} , $T_{\text{Bp}} = e_p T_{\text{eff}}$. The theoretical effective temperature of a soil profile can be estimated as (Ulaby et al., 1986):

$$T_{\text{eff}} = \int_0^{\infty} T(z)\alpha(z)\exp\left[-\int_0^z \alpha(z')dz'\right]dz, \quad (8)$$

where $T(z)$ is the thermodynamic temperature at a depth z , and α is the attenuation coefficient, which is a function of the soil dielectric constant and of the microwave emission wavelength λ . Several simple formulations have been developed to estimate the soil effective temperature from soil properties, and soil moisture and temperature profiles. Choudhury et al. (1982) proposed a parameterisation of T_{eff} based on the soil temperature at deep soil (T_{∞}) corresponding to a depth between 50 cm and 1m, and on a surface temperature (T_{surf}) corresponding to a depth of 0 to 5 cm:

$$T_{\text{eff}} = T_{\infty} + C(T_{\text{surf}} - T_{\infty}). \quad (9)$$

The coefficient C was considered constant for a given frequency, and equal to 0.246 at L-band. On the other hand, Chanzy et al. (1997) presented a model for the soil effective temperature at L- and C-bands based on the air temperature, a deep soil temperature, and the brightness temperature measured at X-band and V-pol. Wigneron et al. (2001) proposed a parameterisation based on (9), but with a coefficient C dependent on the volumetric water content w_s , and two semi-empirical parameters. Another formulation using the soil dielectric constant instead of the volumetric water content was proposed by Holmes et al. (2006). The performance of some of these approaches is analysed in Wigneron et al. (2008). The effect of soil surface roughness on the brightness temperature has been an issue widely addressed in the literature (Choudhury et al., 1979; Wang & Choudhury, 1981; Mo & Schmugge, 1987; Wang, 1983; Wegmüller & Mätzler, 1999; Wigneron et al., 2001; Schneeberger et al., 2004; Escorihuela et al., 2007). Fung (1994) proposes a theoretical physical model based on surface characteristics derived from the measured soil height profile. A simple empirical roughness model which takes into account only the coherent term of the scattering was reported in Choudhury et al. (1979),

$$\Gamma_{s,p} = \Gamma_{s,p}^* \exp\left[-(2k\sigma_s \cos\theta)^2\right], \quad (11)$$

where $\Gamma_{s,p}^*$ is the Fresnel specular reflectivity of soil, k is the electromagnetic wave number, σ_s is the standard deviation of the surface height, and θ is the incidence angle. This model was reviewed, and another formulation was proposed in Wang & Choudhury (1981):

$$\Gamma_{s,p} = \left[(1 - Q_s)\Gamma_{s,p}^* + Q_s\Gamma_{s,q}^*\right]\exp(-h_s \cos\theta^n). \quad (12)$$

In this case, two semi-empirical parameters (h_s and n) were included to model the effects of the polarisation mixing Q_s , and surface roughness. The dependence of these parameters on surface properties such as correlation length or standard deviation of height is not yet clear. Mo & Schmugge (1987) and Wigneron et al. (2001) conclude that the $n=2$ dependence in (12) is too strong for L-band. A value of $n=0$ at both polarisations was found to be consistent with measurements in Wigneron et al. (2001), while Escorihuela et al. (2007) distinguishes n values for both polarisations (1 at horizontal and -1 at vertical). Similarly, there are discrepancies on the value of roughness parameter h_s . Some authors obtain h_s from experimental data by best-fit (Wigneron et al., 2001) while others propose expressions for h_s as a function of geophysical parameters. Mo & Schmugge (1987) obtain good results with two parameterisations of h_s as a function of σ_s and l_c . Finally, there is a general agreement on the value of the cross-polarisation parameter Q_s , which has been found to be very small (0 to 0.12) at L-band.

Apart from these considerations, the effects of frequency and incidence angle on the roughness parameters have not been studied thoroughly. Mo & Schmugge (1987) and Shi et al. (2002) pointed out that the roughness effects depend on both the frequency and the incidence angle. The later suggested a parameterisation of the surface reflectivity derived from data simulated for a wide range of soil water content and roughness properties using the integral equation model (Fung, 1994). The surface reflectivity model of Shi et al. (2002) was tested in Schneeberger et al. (2004) and found not to be capable of explaining discrepancies between the ground truth and remotely sensed data. As a consequence, a new model was developed for describing the influence of the topsoil structure on the L-band emission as an impedance matching between the dielectric constants of soil and air (Mätzler, 2006).

If the remote sensor is placed above a canopy looking downwards, the measured brightness temperature will contain not only information on the soil, but also on vegetation, since vegetation radiates its own energy and, moreover, attenuates and scatters the soil radiation. Chukhlantsev (2006) revises the theory and conducted experimental research over vegetated areas. Although the modelling of the land emission involves analytical solutions of the radiative transfer equation (Ferrazzoli et al., 2002), this approach is not easy to use with experimental data. Hence, the common practice is to use approximate formulas or semi-empirical models in which the different components of the brightness temperature could be differentiated. The brightness temperature of a soil covered by vegetation is usually estimated as the contribution of three terms: (i) the radiation from the soil that is attenuated by the overlying vegetation, (ii) the upward radiation from the vegetation, and (iii) the downward radiation from the vegetation, reflected by the soil, and attenuated by the canopy (Ulaby et al., 1986):

$$T_{B,p}^{\text{model}} = \left(1 + \frac{1 - e_{s,p}}{L_{\text{veg}}} \right) \left(1 - \frac{1}{L_{\text{veg}}} \right) (1 - \omega) T_{\text{veg}} + \frac{e_{s,p}}{L_{\text{veg}}} T_s, \quad (13)$$

where T_{veg} and T_s are the physical temperatures of the vegetation and soil, respectively, $L_{\text{veg}} = \exp(\tau \sec \theta)$ is the attenuation due to the vegetation cover, $\tau = bVWC$ is the optical thickness, b is the b -factor (Van de Griend & Wigneron, 2004), VWC is the vegetation water content, and ω is the single scattering albedo. This formulation is known as the τ - ω model and it is based on the single scattering approach proposed in Kirdiashev et al. (1979). The optical depth is related to the vegetation density and the frequency. The single scattering

albedo describes the scattering of the emitted radiation by the vegetation, and is a function of plant geometry.

3. Soil moisture retrieval algorithms

The brightness temperature of land covers is influenced by many variables, the most important being soil moisture and temperature, and vegetation characteristics. The challenge is to reconstruct the environmental parameters from the measured signal by using a minimum of ancillary data. To do this, different soil moisture retrieval algorithms have been developed. The first one is based on the experimental relationship between the geophysical variables and the radiative transfer equation using a regression technique. This approach has limited applicability, since often the regression is valid only for the test sites where they were obtained. The second approach is based on the use of neural networks. These algorithms have been used with satisfactory results in the retrieval of agricultural parameters from radiometric data (Del Frate et al., 2003), but need a training phase that is not always feasible. The third type of algorithms is widely used and is based on the inversion of radiative transfer models. Obviously, this approach has also disadvantages, since errors of the model lead to errors in the retrieval. The soil moisture models are used as forward models, and the geophysical variables are retrieved by minimisation of a cost function of the type (Wigneron et al., 2003; Pardé et al., 2004; Saleh et al., 2006)

$$F = \sum_{\theta} \frac{(T_{Bh} - T_{Bh}^{\text{meas}})^2}{\sigma_{T_B}^2} + \sum_N \frac{(P_N^{\text{ini}} - P_N)^2}{\sigma_{P_N}^2}. \quad (14)$$

The simulated brightness temperature T_{Bp} is computed using (13), T_{Bp}^{meas} is the measured brightness temperature, and P_N is any of the parameters on which T_{Bp} depends. A first-guess value of the parameter P_N (P_N^{ini}) with associated standard deviation σ_{P_N} can be also considered in the cost function.

4. Soil moisture field experiments

Space missions for Earth observation require a huge amount of previous work to validate the existing science and technology. This is accomplished through airborne or ground-based field experiments. Table 1 summarises some of the campaigns that have been conducted in the last years over land surfaces using L-band radiometers. Most of these radiometers have been designed within the context of preparatory activities previous to a space mission launch.

In the early 70's NASA was getting ready to launch its first microwave radiometers for Earth observations on the Nimbus 5 spacecraft and it needed to learn more about the capabilities of these sensors for land observations. To do this several field campaigns were conducted in the period 1971 to 1973. For the remote sensing of soil moisture irrigated agriculture test areas were selected in the southwestern part of the United States. These experiments demonstrated the sensitivity of microwave radiometers to surface soil moisture and that the longer wavelength sensors worked best (Schmugge et al. 1974; Burke et al., 1979). These data were used to study the effects of surface roughness (Choudhury et al., 1979), soil temperature (Choudhury et al., 1982) and soil texture (Schmugge, 1980). These experiments defined the

basic sensitivity of microwave radiometers for soil moisture sensing and some of the factors affecting this sensitivity. Since that time much has been done to refine and improve this understanding. Some of these later experiments will be described in the following sections. A description of the MOUSE 2004, T-REX 2004/2006, and SMOS REFLEX 2003/2006 campaigns over land carried out by UPC and of their results is provided in the next sections. Radiometric measurements were acquired using the UPC L-band Automatic Radiometer (LAURA), which has a working frequency of 1.4135 GHz, the same as the SMOS payload MIRAS (Villarino, 2004). A view of the experiment sites and the LAURA radiometer is shown in Figure 2.



Fig. 2. Picture of the MOUSE 2004, T-REX 2006, and SMOS REFLEX 2003 experiment sites

Year	Campaign	Site	Surface	Instrument
1971/1975		Phoenix,AZ Imperial valley, CA (USA)	Irrigated agriculture	Multi-frequency Microwave Radiometers
1976/1978	Joint US/USSR exchange	Hand County, SD (USA)	Dryland agriculture	PMIS, MFMR
1985/1989	FIFE	Konza Prairie, Kansas (USA)	Short grass, prairie	PBMR
1990/1991	Monsoon 90	Walnut Gulch AZ (USA)	Desert	PBMR, ESTAR
1992	HAPEX- Sahel	Niger, West Africa	Semi-arid savannah	PBMR
1992/1994	Washita	Oklahoma (USA)	Agricultural	ESTAR, AIRSAR, PBMR
1997/1999	SGP	Oklahoma (USA)	Agricultural	ESTAR, PSR, PAL
1999	ESSC	Reading (UK)	Bare soil	SWaMP-L
2001	INRA	Avignon (FR)	Bare, corn	EMIRAD
2001	EuroSTARSS	Toulouse (FR), Utiel (SP)	Various	STARSS
2002	ETH	Eschikon (CH)	Bare	ELBARA
2002	SMEX	Iowa (USA)	Various	ESTAR, PSR, PALS, AIRSAR
2003/2006	SMOS REFLEX	Utiel (SP)	Vines	LAURA
2003	ELBARA 2003	Wageningen (NL)	Bare, grass	ELBARA
2003-2006	SMOSREX	Toulouse (FR)	Bare, fallow	LEWIS
2003	SMEX	OK,AL,GA(USA)	Various	2DSTAR, PSR, AIRSAR
2004	SMEX	AR, NM (USA)	Various	2DSTAR, PSR

2004	MOUSE	Ispra (IT)	Bare soil	LAURA
2004/2006	T-REX	Agramunt (SP)	Bare soil	LAURA
2004	ETH	Eschikon (CH)	Grass	ELBARA
2004	Bray	Les Landes (FR)	Forest	EMIRAD
2005	ETH	Julich (GE)	Forest	ELBARA
2005	SMEX	Iowa (USA)	Various	APMIR
2005	NAFE	Upper Hunter (AU)	Grass, forest	EMIRAD, PLMR
2006	TuRTLE	El Brull (SP)	Mountain	LAURA
2006/2007	MELBEX	Utiel (SP)	Shrub, vines	EMIRAD
2006	NAFE	Yanco (AU)	Various	PSR, PALS
2007	CLASIC	Oklahoma (USA)	Various	PSR, PALS
2008-2010	GRAJO	Vadillo de la Guareña (SP)	Grass, barley, bare soil	LAURA, SMIGOL

Table 1. Summary of L-band field campaigns over land performed since 1970. Acronyms stand for USA (United States of America), UK (United Kingdom), FR (France), SP (Spain), NL (The Netherlands), CH (Switzerland), GE (Germany), IT (Italy), and AU (Australia).

5. Texture effects on the L-band emissivity of bare soils: the MOUSE 2004 experiment

The Monitoring Underground Soil Experiment (MOUSE) 2004 was performed from day of year (DoY) 159 to 184, 2004, at the Joint Research Centre (JRC) complex of the European Union in Ispra, north of Italy (45°48N, 8°37E; 213 m altitude). The test lane consisted of six 6 m long by 6 m wide by 1 m depth bare plots of different soil types which are distributed along a lane with West-East orientation. The LAURA radiometer, an infra-red video-camera, and the control rack were installed on a metallic gantry guided by a rail on one side and freely rolling on the other. A picture of the setup is shown in Figure 2(c). Soil temperature was measured using 107 probes from Campbell Scientific installed just below the surface, and at 5 cm and 10 cm depth. An infra-red video camera was mounted by LAURA to acquire soil surface temperature images concurrently with the radiometric measurements. Most probably, satellite-borne radiometers will have to rely on this kind of auxiliary sensors to estimate soil moisture from radiometric observations. On the other hand, soil moisture was automatically acquired every 30 min by seven ML2x Thetaprobos per plot installed below the surface (x2), and at 5 cm (x2), 10 cm (x2), and 15 cm (x1). Plots were irrigated three times during the experiment, except RS which was kept dry and protected from water by a sliding tent. Soils at the experiment site were loam (LO), natural sand (SA), sieved sand used in the construction industry (RS), clay from rice fields (CL), a mixture of loam and of commercial products for gardening (OR), and ferromagnetic crushed volcanic soil from Naples (FE).

Figure 3 represents the sensitivity of the H-pol emissivity to the percentage of field capacity, which depends on soil texture. Measurements at 25° (blue), 35° (red), and 45° (green) incidence angles have been plotted. LO, RS, and FE emissivity has a linear dependence on field capacity. The R² estimator at 35° for LO is 71%, for RS 70%, and for FE is 85%. Clay has the worst linear fit, with R² lower than 20%. Soil samples of each plot were acquired and their dielectric constant measured at laboratory (Vall-llossera et al., 2005a).

Soil moisture was retrieved from radiometric measurements using the cost function in (14) with different constraints. The minimum soil moisture RMSE obtained considering different depths as ground-truth data and three different dielectric constant models (Wang &

Schmugge, 1980; Dobson et al., 1985; Vall-llossera et al., 2005a) is represented in Figure 4. Best results for LO and FE are achieved for the soil moisture in the 0 to 5 cm layer, but few discrepancies between RMSE values at different depths were found out. This is mainly due to their almost linear soil moisture profile. Best results for SA were obtained for the soil moisture in the 0-15 cm layer. As sandy soils dry faster, the penetration depth is higher. On the other hand, as RS plot was kept dry throughout the experiment, no important differences in the RMSE have been found in the comparison. Clay had a high water content at 10 cm ($>0.22 \text{ m}^3/\text{m}^3$) and hence the main signal contribution comes from the first 10 cm of soil. Similar RMSE values have been found for OR considering either the 0 to 5 cm layer or the 0 to 10 cm layer as ground-truth. Similarities are because the water content at 5 cm and 10 cm depth is almost the same during the experiment. On the other side, in Figure 4 it can be noted the performance of each dielectric constant models for each soil type. Results for Wang & Schmugge (1980) model are good for loamy and ferromagnetic soils, but their performance for sandy soils is worse than Dobson et al. (1985) and Vall-llossera et al. (2005a). The model in Dobson et al. (1985) offers best results for sandy soils (SA and RS) which registered lower soil moisture values and dried faster than the others. The expressions derived from UPC laboratory experiments show good performance for most of the fields. These facts confirm that the selected dielectric constant model has an impact on soil moisture estimation error and can increase it between 3 to 5% depending on the soil type.

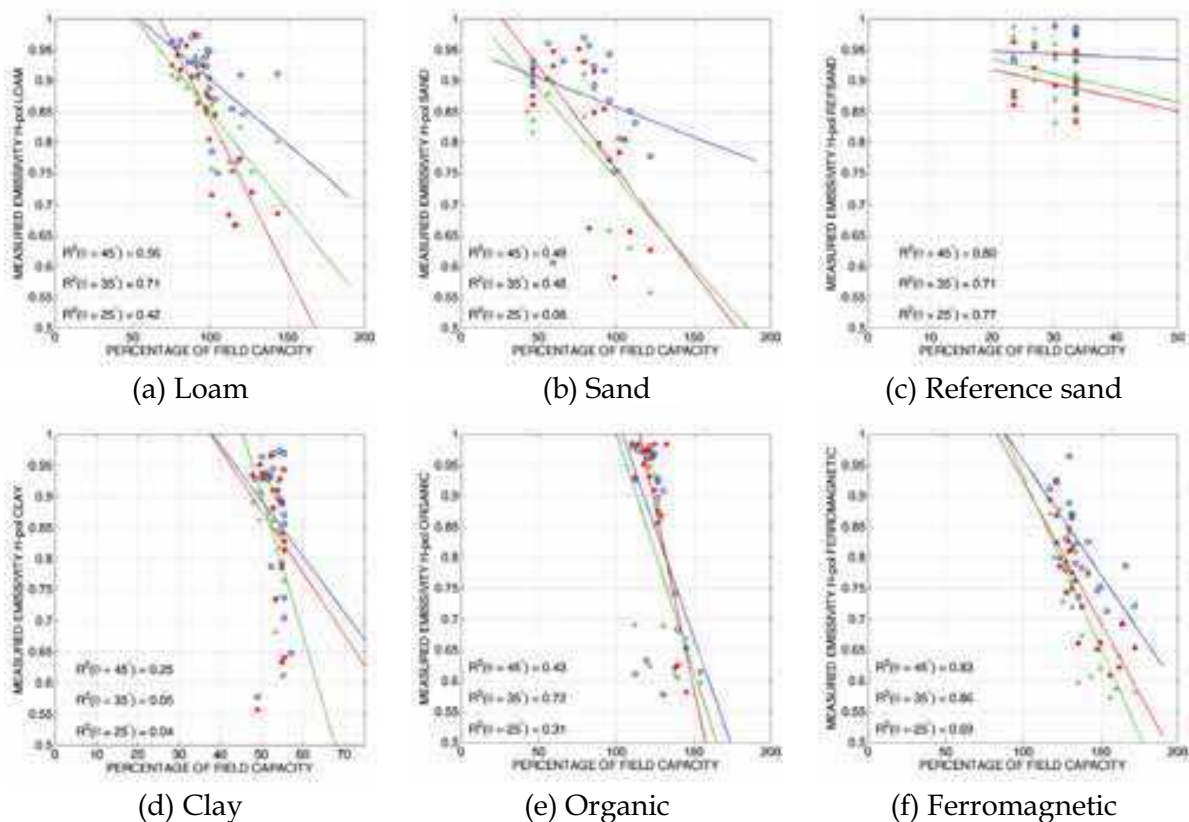
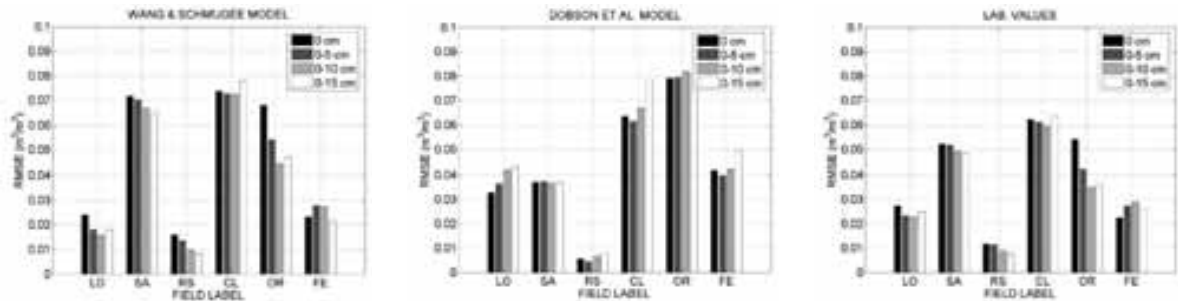


Fig. 3. Variation of the emissivity with the field capacity at H-pol. Colours indicate the incidence angle: 25° (blue), 35° (red), and 45° (green).



(a) Wang & Schumugge

(b) Dobson et al.

(c) Lab. measurements

Fig. 4. Minimum root mean square error of the soil moisture retrieval. Results for a soil dielectric constant model and different soil moisture ground-truth data are represented.

6. Emission of bare rough soils: the T-REX experiments

Several experiments have been performed in the past years to study the L-band emission from bare soils, both at small and large scales. Although small scale measurements are not representative of onboard sensor data, they can be useful to evaluate the various approaches to the land emission modelling. The Terrain-Roughness EXperiments (T-REX) were carried out in Agramunt, Spain (41°48N, 1°7W; 356 m altitude) from DoY 333 to DoY 337, 2004, and then again from DoY 143 to DoY 160, 2006. The sites consisted of bare soil plots with four different ploughing, but the same textural composition (21% clay, 21.3% sand). This section presents some results from the T-REX 2006 experiment. A picture of the site has been shown in Figure 2(a). Each parcel was 6 m x 15 m and the same ploughing was applied to two different plots to observe spatial diversity effects. LAURA was installed on a trailer towed by a car. Radiometric measurements were acquired at incidence angles from 40° to 65° in T-REX 2006, in 5° steps. Every plough type was measured twice each day of experiment.

Parameter (mm)	Plot label			
	A	B	C	D
l_c	126	100	190	96
σ_s	17	16.6	8	33
σ_λ	7	6.8	2.5	17
$h_{\text{air-soil}}$	31	26	13	46

Table 2. Roughness characteristics of the T-REX 2006 ploughs

Roughness measurements were performed in the along and across directions of LAURA's field of view. The standard deviation of height (σ_s) and the correlation length (l_c) of the ploughs at the T-REX 2006 site are summarised in Table 2. Two additional parameters have also been included: (i) $h_{\text{air-soil}}$, which is the transition layer thickness used to evaluate the small-scale soil roughness in the model proposed in Schneeberger et al. (2004), Mätzler (2006, section 4.7) and (ii) σ_λ , which is the standard deviation of height assuming a windowing of length λ . Soil temperature was measured at 0, 5, 10, 15, and 20 cm depth using thermometers. On the other hand, soil moisture was measured with ML2x ThetaProbe sensors at various positions within the radiometer's FOV. As the purpose of this experiment was to study the impact of soil roughness, the site was not irrigated to keep as constant a value of soil moisture as possible. The mean soil moisture during T-REX 2006 was of 4% to 6%.

Figure 5 shows the variation of the emissivity measured during the T-REX 2006 as a function of the incidence angle. Colours indicate the polarisation, H-pol (red) and V-pol (blue), while line styles distinguish the ploughing. While soil emission at H-pol decreases almost linearly with increasing incidence angle (and the trend is more significant at incidence angles above 55°), the emission at V-pol slightly increases with incidence angle until an inflexion point at 55°, when it begins decreasing. Ploughs C and D, which correspond to the smoother and rougher plots in the site, have the highest (lowest) range of variation of the emissivity. The comparison between radiometric measurements and numerical simulations obtained with a numerical approach by means of the integral equation method (IEM; Fung (1994)) are shown in Figure 6. Icons stand for the mean value of LAURA measurements while error bars indicate their standard deviation during the whole T-REX 2006 experiment. Although IEM predicts an increase of the vertical emission with incidence angle, dry soil measurements decrease as incidence angle increases. A good matching between simulations and measurements is observed at horizontal polarisation. The effects of taking into account the incoherent component are only relevant in the case of very rough ploughs (see Figure 6(c), plough D).

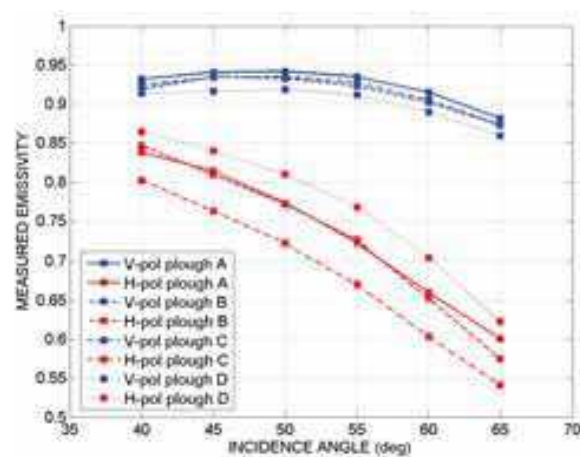


Fig. 5. Variation of the emissivity measured during the T-REX 2006 as a function of the incidence angle for the four ploughs. Colours indicate the polarisation: H-pol (red) and V-pol (blue). Line style and icons distinguish the ploughing.

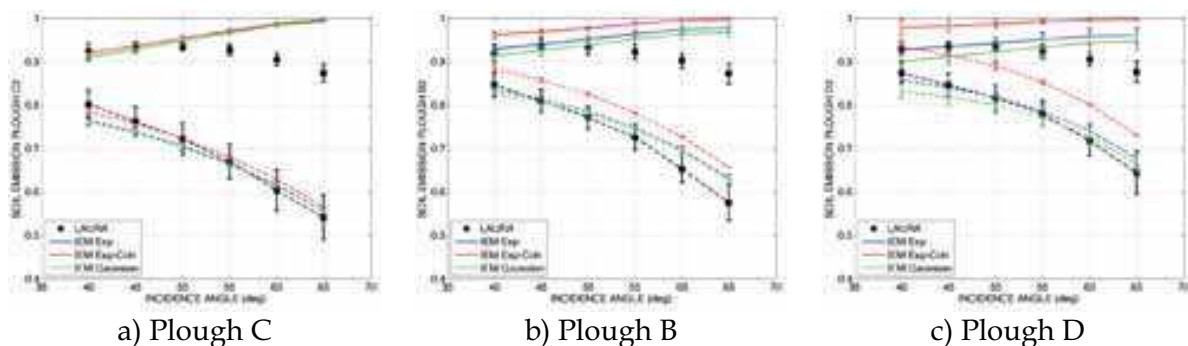


Fig. 6. Variation with time of the emissivity measured during the T-REX 2006 experiment as a function of the incidence angle. The mean value of LAURA measurements (black icons) and their standard deviation during the whole experiment (bars) have been represented together with IEM simulations.

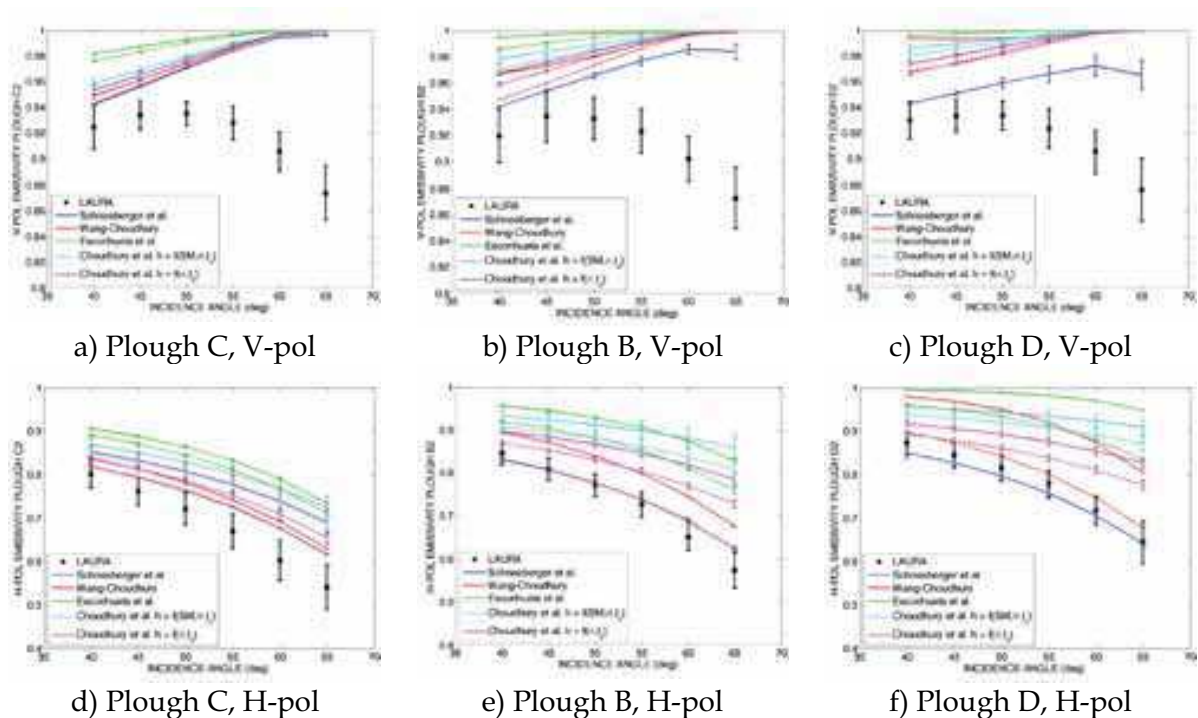


Fig. 7. Comparison between T-REX 2006 measurements (black icons) and the models in Wang & Choudhury (1981), Mätzler (2006, section 4.7), Schneebberger et al. (2004), Mo & Schmugge (1987), and Escorihuela et al. (2007). Solid lines indicate results using the standard deviation of the surface height profile while dashed lines indicates results using the λ -average standard deviation of height

T-REX 2006 measurements were also compared to the semi-empirical soil reflectivity models in Wang & Choudhury (1981), Mo & Schmugge (1987), Escorihuela et al. (2007), and the air-to-soil transition model proposed in Schneebberger et al. (2004). These models propose different expressions for the effective roughness parameter h_s in (12). Results are shown in Figure 7. Upper plots correspond to vertical polarisation while bottom plots correspond to horizontal polarisation. Colours indicate the soil reflectivity model, while line types indicate whether l_c and σ_s of the height profile (solid lines) or their equivalents taking into account the λ -windowing (dashed lines) have been used. Both the model in Wang & Choudhury (1981) using as inputs the λ -windowing soil roughness characteristics and the air-to-soil transition model from Schneebberger et al. (2004) fit data. However, Schneebberger et al. (2004) does not fit T-REX 2006 measurements of wet soil, which suggests that inhomogeneities in soil moisture or the presence of dew make it difficult to properly characterise the upper soil layer, which is needed for the air-to-soil transition model.

7. Radiometric observations of fully developed vines

Several papers are available that present experimental studies of brightness temperatures from vegetation canopies (Jackson et al. 1982; Jackson et al., 1991; Ferrazzoli et al., 2002; Van de Griend & Wigneron, 2004; Saleh et al., 2006). A look at the field experiments conducted during the past decades over vegetated sites shows how they focused their attention on crops such as alfalfa, wheat corn, or soybean, on grass, on forests, and on bushes, but few

studies had been conducted over vineyards. In this context, two ground-based field experiments were performed to study the variations on the emissivity due to vines development. The SMOS REFERENCE pixel L-band EXperiments (REFLEX) were carried out in July 2003 and then again from July to November 2006 at two vineyards within the València Anchor Station (VAS; Figure 2(b)), Spain (Vall-llossera et al., 2005b). The VAS has been selected as a SMOS Cal/Val site because of its almost homogeneous land cover (vineyards) and its size, which is approximately that of a SMOS pixel. The goal of the SMOS REFLEX experiments was to assess the impact of grapevines on the radiometric emission and on the sensitivity of the sensor to soil moisture. Results from the SMOS REFLEX 2003 experiment are presented hereafter.

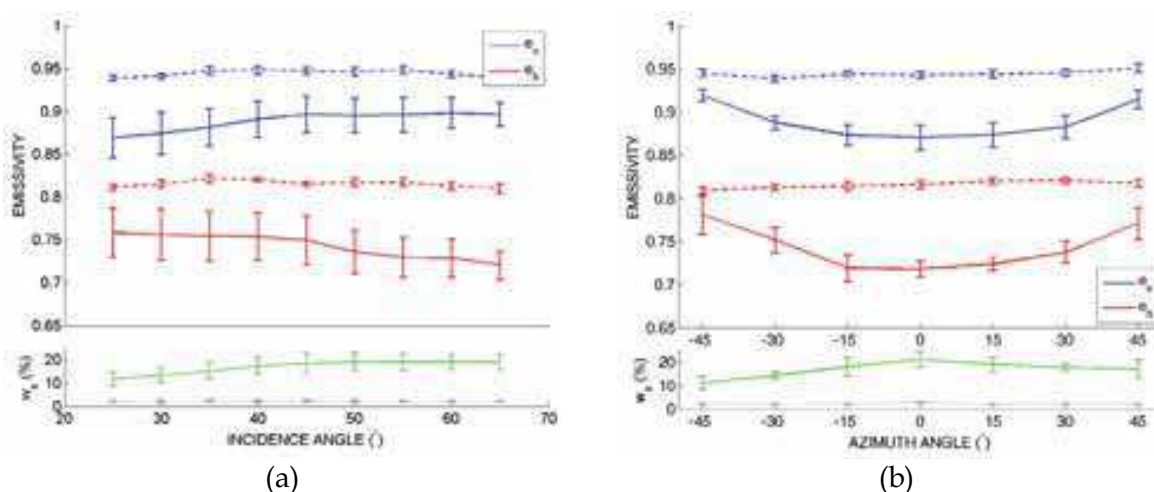


Fig. 8. Mean value and standard deviation of the emissivity and of the ground-truth soil moisture as a function of (a) the incidence angle and for all azimuth angles, and (b) the azimuth angle and for all incidence angles. DoY 185 (solid line, wet soil) and DoY 181 (dashed-dotted line, dry soil) have been represented. Blue and red indicate vertical and horizontal polarisations, respectively.

During SMOS REFLEX 2003 radiometric measurements were acquired from DoY 181 to 191 at nine incidence angles (from 25° to 65° in 5° steps) and seven azimuth angles. Pictures at every look direction were taken to estimate the percentage of FOV covered by plants. The site was irrigated until saturation on DoY 182 and 185, and then was let to dry out. Even though the field was irrigated until saturation, different soil moisture values were measured depending on the location of the test point within the vineyard. This is most probably because of surface inhomogeneities and variations on the compactness of the terrain due to plough and roots distribution. This large spatial variability in soil moisture, which in this case varies from 3% up to 35% in a 20 m x 20 m area, is one of the main problems soil moisture retrieval algorithms must face since it complicates the comparison between ground-truth and estimated w_s at the plot scale. Volumetric soil moisture, soil temperature, and soil roughness were measured, and plants were fully characterised.

Figure 8(a) represents the mean value and standard deviation of the emissivity and of the ground-truth soil moisture as a function of the incidence angle and for all azimuth angles. Measurements from DoY 185 (solid line) and DoY 181 (dashed-dotted line) have been represented. The mean value of both polarisations seems independent of incidence angle for

completely dry soils, which is the case of DoY 181, being the std. of measurements lower than 0.005 (0.01) in emissivity -1.5 K (3 K) in brightness temperature- for vertical (horizontal) polarisations. In contrast, for wet soil an ascending trend is observed for V-pol emissivity up to 45°, when V-pol emissivity seems to saturate, while H-pol emissivity decreases as incidence angle increases. The std. of measurements for wet soils is 0.025 (0.03) for vertical (horizontal) polarisations.

The mean value and standard deviation of the emissivity from DoY 181 and DoY 185 as a function of the azimuth angle and for all incidence angles is represented in Figure 8(b). For dry soils no dependence on the azimuth angle is observed, being the standard deviation of measurements lower than 1.5 K at both polarisations. In the case of wet soils, and since the contribution from vines is supposed to be the same for specular azimuth angles with respect to zero, the inhomogeneity in soil moisture content, which is higher for positive azimuth angles, leads to an asymmetry in the emission measurements of DoY 185 (solid lines), which as expected are higher for the lowest soil moisture. For a given azimuth angle, the standard deviation of the measured emissivity at V-pol goes from 0.014 (4 K) at 0° down to 0.008 (2 K) at 65°, whereas the largest standard deviation at H-pol goes from 0.007 (2.6 K) at 0° up to 0.022 (7 K) at 45°.

Figure 9(a) shows the variation of the retrieved albedo with respect to the incidence angle for all azimuth angles. Icons indicate the day of experiment, while the solid line is the mean value of the whole experiment at each incidence angle. The albedo is smaller than 0.15, having its maximum for an incidence angle of 35° and then decreasing as the incidence angle increases. On the other hand, the opacity tends to increase with incidence angle as shown in Figure 9(b) which is in accordance to the higher fraction of area covered by vegetation as the incidence angle. Good agreement between measured and computed values is appreciated for incidence angles below 55°. For 55° the algorithm does not always converge and at 60° and 65°, the convergence is rarely achieved, pointing out a problem in the emissivity model function for large incidence angles. This discrepancy can be due to the fact that as the incidence angle increases, the signal from the soil suffers from more attenuation and scattering in the canopy. The $\tau-\omega$ model is a valid and simple forward model to be used in optimal estimation approaches, but improvements are required if it is to be used at high incidence angles.

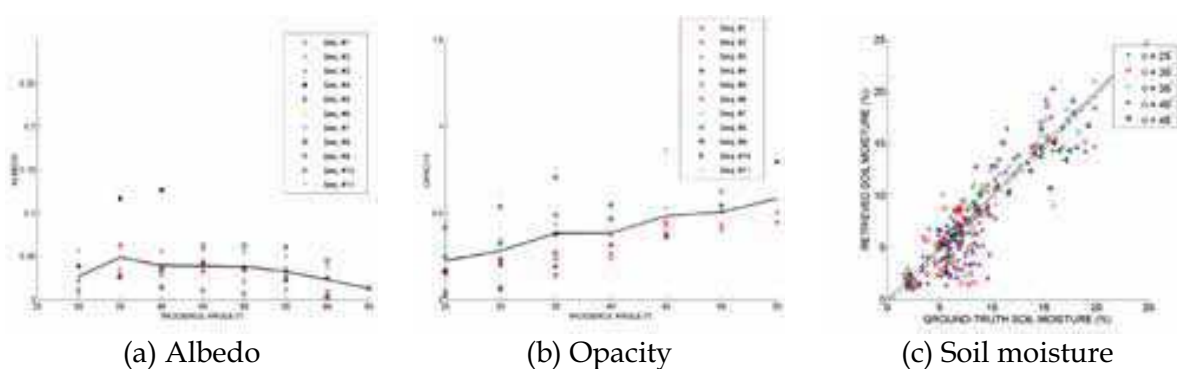


Fig. 9. Dependence of the retrieved vegetation albedo (a), and opacity (b) on the incidence angle. Icons represent the value estimated from LAURA measurements for each day of experiment and all azimuth angles. The mean value is represented with a black solid line. (c) Ground truth soil moisture vs. estimates from radiometric measurements.

In order to retrieve the soil water content from the LAURA's measurements, an iterative algorithm, based on the least squares minimisation procedure, was applied. A better performance was found out when the albedo, opacity and soil moisture were simultaneously retrieved using (14). The first guesses for the opacity and the albedo are the estimated values obtained in the iterative algorithm described before. The algorithm converges for incidence angles equal to or smaller than 50° , only for some day of experiments at 55° , and rarely for 60° or 65° due to the increasing discrepancy between the model and the data as the incidence angle increases. When the incidence angle increases, the canopy influence becomes more important (higher attenuation on the signal and higher scattering contribution), so a higher order approximation for the direct model becomes necessary. In Figure 9(c), the soil moisture estimated from LAURA data is compared to ground-truth soil moisture data. The slope of the computed linear regression is 0.9 (close to 1), which shows a good agreement between both values. The error between estimations and measurements is about 2.3%, which is smaller than the 4% accuracy required for SMOS.

8. Conclusions

The basics of land emission modelling have been summarised in this chapter, and an overview of the field experiments over land carried out during the last three decades has been given to present to the reader the state of the art. Some results of the recent SMOS REFLEX 2003, MOUSE 2004, and T-REX 2006 experiments have been reported here. These are, among others, part of the preparatory experiments for the SMOS mission, which in the near future will provide soil moisture maps at global scale.

Soil texture influences the electromagnetic behaviour of soils since it affects their dielectric constant. During MOUSE 2004, six types of bare soils with different soil moisture contents were measured at five incidence angles. As expected, variations on the moisture profile were noted depending on texture. The emission of loams and sands showed a linear dependence on the percentage of field capacity, especially at H-pol. In this case, the R-squared estimator at 35° was found to be between 70% and 85%. On the contrary, clay showed no linear trend which, however, can not be a general conclusion since clay data had a large scattering.

The modified Wang & Choudhury (1981) soil emission model, with $Q_s=0$ and $n=0$, was used as forward model in the soil moisture retrieval algorithm. Best results were obtained when no constraints were applied to soil moisture and temperature. The estimated soil moisture was compared with the soil moisture measured at different depths. For loam and ferromagnetic soils best results were achieved considering as ground-truth data the soil moisture in the 0 to 5 cm layer, 0 to 15 cm layer for sands, and 0 to 10 cm layer for clays. On the other hand, when results for every dielectric constant model were compared, it was found out that the Wang & Schmugge (1980) model had a better performance in the retrieval algorithm of loam and ferromagnetic soils, while the Dobson et al. (1985) model offered best results for sands.

Results from MOUSE 2004 suggest that the soil dielectric constant model should be selected as a function of texture, since the root mean squared error can vary from 2% to 7% depending on the soil texture, and that soil moisture estimates will be the averaged value in a soil layer which will depend on texture.

Soil roughness has a strong impact on land brightness temperature. This effect is more noticeable in the case of dry soils. Data from bare soils with a standard deviation of height varying from 8 mm to 33 mm was acquired during the T-REX experiments, and was compared to predictions from numerical and semi-empirical soil emission models. The goodness of these models is of key importance for an accurate soil moisture estimation from satellite data. As expected, dry soil emissivity at H-pol decreased almost linearly with increasing incidence angle, being the decrement inversely proportional to soil roughness. Although similar emission was measured at H-pol for all plough at low incidence angles, it was noted that emission decreases slowly for rough soils than for smooth soils. Above an incidence angle of 50° , the decreasing slope of H-pol emission was higher for all plough. The sensitivity of V-pol to roughness is lower than that of H-pol. The trend of V-pol emission was found to be different depending on whether the soil was wet or dry. When the soil is wet the emission increased with the incidence angle, which is in accordance with most model predictions. However, the trend for dry soils is decreasing with increasing incidence angle and roughness. This may suggest the existence of a relationship between soil moisture and the effective roughness.

The integral equation method (IEM) predicts an increase in V-pol emission with incidence angle, which is not in accordance with measurements of dry soils. On the other hand, the predicted descending trend at H-pol with increasing incidence angle is in accordance to measurements, although IEM underestimates the soil emission both for dry and wet soils. In a randomly ploughed field, without a significant tillage direction, the impact of choosing an exponential or gaussian height probability density function in the IEM model is minimum, whereas it was noted that the incoherent term of the reflectivity must be considered for rough soils.

In general, all semi-empirical land emission models follow the trend of dry soils measurements at H-pol, whereas discrepancies exist for wet soils. Neither the semi-empirical models nor the IEM describe the trend of dry soils V-pol measurements, being the error at this polarisation larger as the incidence angle increases. The lowest error between predictions and measurements for H-pol was obtained using the Wang & Choudhury (1981) model, but with roughness statistics averaged as a function of the measurements wavelength. The dependence on the incidence angle proposed by Wang & Choudhury (a squared cosine) had been discussed by other authors who considered it to be too much strong at L-band. However, this simple formulation has been tested with T-REX data with good results if the averaged standard deviation in transects equal to the wavelength is used. The SMOS REFLEX 2003/2006 experiments site was in the Valencia Anchor Station, a selected area for the SMOS calibration and validation activities. No previous studies over vines were reported in the literature prior to these campaigns. In the first experiment, fully developed vines were characterised during two weeks, while controlled irrigations moistened the field. The second experiment was planned to monitor changes in the L-band emission of vineyards during different stages of plants development.

Since vines do not have a predominant vertical nor horizontal structure, the opacity and the albedo were found to be independent on the polarisation. The Wang & Choudhury (1981) model was used as the soil emission forward model in the retrieval algorithm, while the dielectric constant model was the one from Wang & Schmugge (1980). Good results were obtained for incidence angles up to 55° , but the convergence of the algorithm was rarely achieved above that value. The error between ground-truth and estimated soil moisture was

2.3%, better than the 4% required for SMOS. For incidence angles above 55° the convergence of the algorithm was rarely achieved, probably due to the larger effect of the vegetation at large incidence angles, not accurately described by the model. Higher order models should be accounted for at these angles.

Although the radiometric behaviour varies from one canopy to the other, at a larger scale such as that of SMOS it is very likely that the vegetation types can be averaged over the footprint and that it is not necessary to account for an accurate distinction between canopies.

9. Acknowledgements

A. Monerris would like to thank Spanish Ministry of Science and Education projects MIDAS-2 ESP2002-11648-E, MIDAS-3 ESP2004-00671, and MIDAS-4 ESP2005-06823-C05-02, for funding the SMOS REFLEX, T-REX and MOUSE 2004 field experiments, and the FPU AP2003-1567 grant. Special thanks are also given to M. Vall-llossera and A. Camps, from UPC, for their valuable comments during the analysis of the experimental data.

10. References

- Barré, H., Duesmann, B. & Kerr, Y.H. (2008). SMOS: The mission and the system. *IEEE Trans. Geosci. and Remote Sens.*, 46, 587-593
- Behari, J. (2005). *Microwave dielectric behaviour of wet soils (Remote Sensing and Digital Image Processing)*, Springer, ISBN-10:1402032714, The Netherlands
- Brady, N.C. & Weil, R.R. (2003). *Elements of the nature and properties of soils*, 2nd ed., Prentice Hall, ISBN-10:013048038X, NJ, USA
- Burke, W. J., Schmugge, T. J. & Paris, J.F. (1979). Comparison of 2.8 and 21 cm microwave radiometer observations over soils with emission model calculations, *J. Geophys. Res.*, 84, 287-294.
- Chanzy, A., Raju, S. & Wigneron, J.-P. (1997). Estimation of soil microwave effective temperature at L and C bands. *IEEE Trans. Geosci. and Remote Sens.*, 35, 3, 570-580
- Choudhury, B.J., Schmugge, T.J., Chang, A.T.C. & Newton, R.W. (1979). Effect of surface roughness on the microwave emission of soils. *J. Geophys. Res.*, 84, 5699-5705
- Choudhury, B.J., Schmugge, T.J. & Mo, T. (1982). A simple parameterization of effective soil temperature for microwave emission. *J. Geophys. Res.*, Vol., No., (month and year of the edition) 1301-1304
- Chukhlantsev, A.A. (2006). *Microwave radiometry of vegetation canopies*, Springer, ISBN-10 1-4020-4681-2, The Netherlands
- Del Frate, F., Ferrazzoli, P. & Schiavon, G. (2003). Retrieving soil moisture and agricultural variables by microwave radiometry using neural networks. *Rem. Sens. Env.*, 84, 2, 174-183
- Dobson, M. C., Ulaby, F. T., Hallikainen, M. T. & Elrayes, M. A. (1985). Microwave dielectric behaviour of wet soils 2. Dielectric mixing models. *IEEE Trans. Geosci. and Remote Sens.*, 23, 35-46
- Eagleman, J.R. & Lin, W.C. (1976). Remote sensing of soil moisture by a 21 cm passive radiometer. *J. Geophys. Res.*, 81, 3660-3666
- Entekhabi, D., Njoku, E., Houser, P., Spencer, M., Doiron, T., Smith, J., Girard, R., Belair, S., Crow, W., Jackson, T., Kerr, Y., Kimball, J., Koster, R., McDonald, K., O'Neill, P.,

- Pultz, T., Runnig, S., Shi, J., Wood, E. & van Zyl, J. (2004). The Hydrosphere State (HYDROS) mission concept: An Earth system pathfinder for global mapping of soil moisture and land freeze/thaw. *IEEE Trans. Geosci. and Remote Sens.*, 42, 2184-2195
- Escorihuela, M.J., Kerr, Y.H., de Rosnay, P., Wigneron, J.-P., Calvet, J.-C. & Lemaitre, F. (2007). A simple model of the bare soil microwave emission at L-band, *IEEE Trans. Geosci. and Remote Sens.*, 45, 1978-1987
- Ferrazzoli, P., Guerriero, L. & Wigneron, J.-P. (2002). Simulating L-band emission of forests in view of future satellite applications. *IEEE Trans. Geosci. and Remote Sens.*, 40, 2700-2708
- Fung, A.K. (1994). *Microwave Scattering and Emission. Models and their applications*, Artech House, ISBN-10:0890065233, Norwood, MA.
- Hallikainen, M.T., Ulaby, F.T., Dobson, M.C., El-Rayes, M.A. & Wu, L. (1985). Microwave dielectric behaviour of wet soil - Part 1: Empirical models and experimental observations. *IEEE Trans. Geosci. and Remote Sens.*, GE-23, 25-34
- Hipp, J.E. (1974). Soil electromagnetic parameters as a function of frequency, soil density and soil moisture, *Proceedings of IEEE*, 98-103
- Holmes, T., de Rosnay, P., de Jeu, R., Wigneron, J.-P., Kerr, Y., Calvet, J.-C., Escorihuela, M.J., Saleh, K. & Lemaitre, F. (2006). A new parameterization of the effective temperature for L-band radiometry. *Geophys. Res. Lett.*, 33, 7405
- Jackson, T.J., Schmugge, T.J. & Wang, J.R. (1982). Passive microwave sensing of soil moisture under vegetation canopies. *Water Resources Research*, 18, 1137-1142
- Jackson, T.J. & Schmugge, T.J. (1989). Passive microwave remote sensing system for soil moisture: Some supporting research. *IEEE Trans. Geosci. and Remote Sens.*, 27, 2, 225-235
- Jackson, T. J. & Schmugge, T. J. (1991). Vegetation effects on the microwave emission from soils. *Remote Sens. Environ.*, 36, 203-212
- Kerr, Y.H., Waldteufel, P., Wigneron, J.-P., Martinuzzi, J.M., Font, J. & Berger, M. (2001). Soil moisture retrieval from space: the Soil Moisture and Ocean Salinity (SMOS) mission. *IEEE Trans. Geosci. and Remote Sens.*, 39, 1729-1735
- Kirdiashev, K.P., Chukhlantsev, A.A., & Shutko, A.M. (1979). Microwave radiation of the Earth's surface in the presence of vegetation cover. *Radio Eng. Electron. Phys.*, 2, 37-56.
- Koster, R.D., Dirmeyer, P.A., Guo, Z., Bonan, G., Chan, E., et al. (2004). Regions of strong coupling between soil moisture and precipitation. *Science*, 305, 5687, 1138-1140
- Mätzler, C. & Standley, A. (2000). Relief effects for passive microwave remote sensing, *J. Geophys. Res.*, 21, 2403-2412
- Mätzler, C. (2006). *Thermal Microwave Radiation: Applications for Remote Sensing*, IET Electromagnetic Waves Series 52, ISBN-10:0863415733, London, UK
- McMullan, K.D., Brown, M.A., Martín-Neira, M., Rits, W., Martí, J. & Lemanczyk, J. (2008). SMOS: The payload. *IEEE Trans. Geosci. and Remote Sens.*, 46, 3, 594-605
- Mironov, V.L., Dobson, M.C., Kaupp, V.H., Komarov, S.A. & Kleshchenko, V.N. (2004). Generalized refractive mixing dielectric model for moist soils. *IEEE Trans. Geosci. and Remote Sens.*, 42, 4, 773-785
- Mo, T. & Schmugge, T. (1987). A parameterization of the effect of surface roughness on microwave emission, *IEEE Trans. Geosci. and Remote Sens.*, 25, 47-54

- Monerris, A., Benedicto, P., Vall-llossera, M., Santanach, E., Piles, M. & Prehn, R. (2008). Assessment of the topography impact on microwave radiometry at L-band. *J. Geophys. Res.*, 113(B12202)
- Pardé, M., Wigneron, J.-P., Waldteufel, P., Kerr, Y.H., Chanzy, A., Sobaerg, S.S. & Skou, N. (2004). N-parameter retrievals from L-band microwave observations acquired over a variety of crop fields. *IEEE Trans. Geosci. and Remote Sens.*, 42, 6, 1168-1178
- Roth, C.H., Malicki, M.A. & Plagge, R. (1992). Empirical evaluation of the relationship between soil dielectric constant and volumetric water content as the basis for calibrating soil moisture measurements by TDR. *J. of Soil Sci.*, 43, 1-3
- Saleh, K., Wigneron, J.-P., de Rosnay, P., Calvet, J.-C., Escorihuela, M.J., Kerr, Y. & Waldteufel, P. (2006). Impact of rain interception by vegetation and mulch on the L-band emission of natural grass. *Remote Sens. Environ.*, 101, 127-139
- Schmugge T., P. Gloersen, T. T. Wilheit, and F. Geiger, 1974. Remote Sensing of Soil Moisture with Microwave Radiometers, NASA/GSFC X-652-72-305, Jour. Geophys. Res., 79(2), pp. 317-323.
- Schmugge, T. J. 1980. Effect of Texture on the Microwave Emission from Soils, NASA Tech. Memo. 80632, *IEEE Trans. on Geoscience and Remote Sensing*, GE-18, pp. 353-361.
- Schneeberger, K., Schwank, M., Stamm, Ch., de Rosnay, P., Mätzler, Ch. & Flüher, H. (2004). Topsoil structure influencing soil water retrieval by microwave radiometry. *Vadose Zone Journal*, 3, 1169-1179
- Schwank, M., Stähli, M., Wydler, H., Leuenberger, J., Mätzler, C. & Flüher, H. (2004). Microwave L-band emission of freezing soil, *IEEE Trans. Geosci. and Remote Sens.*, 42, 1252-1261
- Talone, M., Camps, A., Monerris, A., Vall-llossera, M., Ferrazzoli, P. & Piles, M. (2007). Surface topography and mixed pixel effects on the simulated L-band brightness temperatures, *IEEE Trans. Geosci. and Remote Sens.*, 42, 786-794
- Topp, G.C., Davies, J.L. & Annan, A.P. (1980). Electromagnetic determination of soil water content: Measurements in coaxial transmission lines. *Water Resour. Res.*, 16, 574-582
- Ulaby, F.T., Moore, R.K. & Fung, A.K. (1986). *Microwave Remote Sensing: Active and Passive, vol. II, Radar remote sensing and surface scattering and emission theory*, Addison-Wesley, ISBN-10:0890061912, NY
- Van de Griend, A. A. & Wigneron, J. P. (2004). The *b*-factor as a function of frequency and canopy type at H-polarization. *IEEE Trans. Geosci. and Remote Sens.*, 42, 4, 786-794
- Vall-llossera, M., Cardona, M., Blanch, S., Camps, A., Monerris, A., Corbella, I., Torres, F. & Duffo, N. (2005a). L-band dielectric properties of different soil types collected during the MOUSE 2004 field experiment. *Proceedings IGARSS*, 2, 1109-1112
- Vall-llossera, M., Camps, A., Corbella, I., Torres, F., Duffo, N., Monerris, A., Sabia, R., Selva, D., Antolín, C., López-Baeza, E., Ferrer, J.F. & Saleh, K. (2005b). SMOS REFLEX 2003: L-band emissivity characterization of vineyards. *IEEE Trans. Geosci. and Remote Sens.*, 43, 5, 973-982
- Villarino, R. (2004). *Empirical Determination of the Sea Surface Emissivity at L-band: A contribution to ESA's SMOS Earth Explorer Mission*. Ph.D. thesis, RSLab, UPC. [Online] <http://www.tesisenxarxa.net/TDX-1019104-170028/index.html>
- Wang, J.R. & Schmugge, T.J. (1980). An empirical model for the complex dielectric permittivity of soils as a function of water content. *IEEE Trans. Geosci. and Remote Sens.*, 18, 288-295

- Wang, J.R. (1983). Passive microwave sensing of soil moisture content: The effects of soil bulk density and surface roughness. *Remote Sens. Environ.*, 13, 329-344
- Wang, J.R. & Choudhury, B.J. (1981). Remote sensing of soil moisture content over bare field at 1.4 GHz frequency. *J. Geophys. Res.*, 86, 5277-5282
- Wegmüller, U. & Mätzler, C. (1999). Rough bare soil reflectivity model. *IEEE Trans. Geosci. and Remote Sens.*, 37, 1391-1395
- Wigneron, J., Laguerre, L. & Kerr, Y.H. (2001). A simple parameterization of the L-band microwave emission from rough agricultural soils. *IEEE Trans. Geosci. and Remote Sens.*, 39, 1697-1707
- Wigneron, J.-P., Calvet, J.-C., Pellarin, T., de Griend, A.A. Van, Berger, M. & Ferrazzoli, P. (2003). Retrieving near-surface soil moisture from microwave radiometric observations: current status and future plans. *Remote Sens. Environ.*, 85, 489-506
- Wigneron, J.-P., Chanzy, A., de Rosnay, P., Rüdiger, C. & Calvet, J.-C. (2008). Estimating the effective soil temperature at L-band as a function of soil properties. *IEEE Trans. Geosci. And Remote Sens.*, 46, 3, 797-807



Advances in Geoscience and Remote Sensing

Edited by Gary Jedlovec

ISBN 978-953-307-005-6

Hard cover, 742 pages

Publisher InTech

Published online 01, October, 2009

Published in print edition October, 2009

Remote sensing is the acquisition of information of an object or phenomenon, by the use of either recording or real-time sensing device(s), that is not in physical or intimate contact with the object (such as by way of aircraft, spacecraft, satellite, buoy, or ship). In practice, remote sensing is the stand-off collection through the use of a variety of devices for gathering information on a given object or area. Human existence is dependent on our ability to understand, utilize, manage and maintain the environment we live in - Geoscience is the science that seeks to achieve these goals. This book is a collection of contributions from world-class scientists, engineers and educators engaged in the fields of geoscience and remote sensing.

How to reference

In order to correctly reference this scholarly work, feel free to copy and paste the following:

Alessandra Monerris and Thomas Schmugge (2009). Soil moisture estimation using L-band radiometry, *Advances in Geoscience and Remote Sensing*, Gary Jedlovec (Ed.), ISBN: 978-953-307-005-6, InTech, Available from: <http://www.intechopen.com/books/advances-in-geoscience-and-remote-sensing/soil-moisture-estimation-using-l-band-radiometry>

INTECH
open science | open minds

InTech Europe

University Campus STeP Ri
Slavka Krautzeka 83/A
51000 Rijeka, Croatia
Phone: +385 (51) 770 447
Fax: +385 (51) 686 166
www.intechopen.com

InTech China

Unit 405, Office Block, Hotel Equatorial Shanghai
No.65, Yan An Road (West), Shanghai, 200040, China
中国上海市延安西路65号上海国际贵都大饭店办公楼405单元
Phone: +86-21-62489820
Fax: +86-21-62489821

© 2009 The Author(s). Licensee IntechOpen. This chapter is distributed under the terms of the [Creative Commons Attribution-NonCommercial-ShareAlike-3.0 License](https://creativecommons.org/licenses/by-nc-sa/3.0/), which permits use, distribution and reproduction for non-commercial purposes, provided the original is properly cited and derivative works building on this content are distributed under the same license.

IntechOpen

IntechOpen